G. A. Acosta-Fernandez[1,2], N. M. Castrejon-Esparza[1,2], S. Morales-Inzunza[1,2], K.E. Martinez-Torres[1,2], L.A. Vargas-Robles[3], M.E. Gonzalez-Trevizo[1,2]*

Utilizing Satellite Remote Sensing and Geographic Information Systems for Assessing Urban Heat Island Effects as Urban Planning Tools for Emerging Economies

[1]Universidad Autónoma de Baja California, Facultad de Ingeniería Arquitectura y Diseño, C. Transpeninsular Ensenada - Tijuana 3917, 22860, Ensenada, México.
[2]PRISMA Research Group, C. Transpeninsular Ensenada - Tijuana 3917, 22860, Ensenada, México.
[3]Universidad Iberoamericana León, Departamento de Arquitectura y Diseño, Blvd. Jorge Vértiz Campero 1640, 37238, León, México.

Abstract

This research investigates the use of remote sensing methods to assess the Surface Urban Heat Island (SUHI) phenomenon in an emerging economy city with a Mediterranean climate by using a case study of Ensenada, Mexico, specifically analyzing data from the years 2019 and 2023. With the increase in urban populations, especially in developing countries, the effects of urbanization on climate, energy, and health become more crucial. The research utilizes Landsat 8 satellite spectral images to evaluate variations in Land Surface Temperature (LST) and urban heat island intensity. Employing the Normalized Difference Vegetation Index (NDVI), the research uncovers substantial temperature elevations, with an average increase of 1.5 °C affecting 42.37% of the city. The northeastern region experienced significant temperature fluctuations, driven by the growth of urban areas and the decrease in green infrastructure. The research emphasizes the need to include green infrastructure, such as parks and green roofs, in urban planning to alleviate urban overheating impacts. Furthermore, it emphasizes the need for ongoing surveillance via Geographic Information Systems (GIS) and remote sensing to direct sustainable city growth. These results provide practical insights for urban planners, government authorities, and private sector stakeholders to create policies that seek to reduce heat-related vulnerabilities.

***Keywords**: Surface Urban Heat Island, Land Surface Temperature, Urban planning, Heat vulnerability, Remote sensing*

1. Introduction

In 2022, the worldwide urban population was roughly anticipated to be about 4.5 billion, accounting for 56.9% of the overall population. Urban regions record continuous growth, and by 2050, more than 70% of the global is anticipated to be located in urban centers, mostly driven by Less Developed Regions (LDR) or emerging economies [1], where five out of six people live in social and economic inequities and lack of regulation. In this context, Latin America is projected to have substantial urban expansion, which might result in an additional 53 million people living in metropolitan areas by 2035 [2].

The majority of urban land development is expected to take place in low-income nations. If not properly planned, urban sprawl might become a pressing worldwide concern. Small cities and towns with a population of 250,000 people play a crucial role in creating sustainable urban futures in low-income nations. Therefore, it is necessary to improve planning capacity, particularly for emerging cities facing challenges such as high population density, lack of access to energy, and inequality. These issues are urgent global aspects that need immediate attention. According to the UN World City report, "*A multidimensional approach is key to an inclusive urban future*" [3].

Urbanization affects attempts to mitigate climate change by contributing to land cover degradation via extensive deforestation. At the same time, urban atmospheric air quality is affected by the modification of land through construction materials. This modification alters the normal thermal storage, radiative, and turbulent heat transfer, as well as the sensible heat flux [4]. These changes result from the thermal and optical properties of the materials used and from the lower evaporative cooling of infrastructures with low emissivity [5]. These factors contribute to increased human exposure to the negative effects of global warming at the local scale [6]. The higher albedo and Land Surface Temperature (LST) of urban areas compared to their natural surroundings, along with the impact of urban geometry, anthropogenic heat, and the region's geographical and microclimatic conditions, influence the thermal balance of the urban environment. The multivariable phenomenon is the main cause of the exacerbation of the Urban Heat Island Intensity (UHII) [7], [8].

In the climate change context, science-based urban planning is undeniably advantageous for reducing urban overheating and its effects on human vulnerability caused by global warming [9], thus the spatiotemporal evolution in urban microclimate has a serious effect on environmental heterogeneity, and urban policies to address this urgent topic must be developed [10]. Satellite remote sensing is a valuable method for sustainable urban planning, particularly in addressing the Urban Heat Island (UHI) phenomenon through the analysis of multiple indices, and socio-demographic, and environmental approaches such as Local Climate Zones (LCZ), which allow associating the characteristics of the urban environment with Land

Surface Temperature and identifying patterns during the day, enabling urban planners to classify metropolitan areas by examining building geometry and land cover using satellite data from numerous sources [11]. Multiple studies have shown the existence of temperature changes during the day, which may be accurately observed by analyzing data from Landsat and ASTER satellites. Moreover, the configuration and composition of Land Use and Land Cover (LULC), and cover materials have a significant impact on LST, such as the findings found by Ejiagha [12] where it was identified that residential and industrial areas were the largest contributors to LST during 2015 and 2018, increasing LST by up to 6.95 °C. In addition, the combination of remote sensing and spatial network analysis can provide useful insights into the impact of various urban areas such as the findings presented by Mohamed [13]. Governments around are implementing green city strategies to transform obstacles into possibilities. Saudi Vision 2030 advocates for intelligent development to enhance the economy while safeguarding natural resources. The urban heat island (UHI) - who performed a comparison of LST between two districts in Saudi Arabia, finding that the Al-Shrashef district whose main spatial characteristic is the compact urban fabric presents a lower LST up to 1 °C compared to the Al Eskan district which presents large tracts of open space. On the other hand, Jato-Espino [14] developed ArcUHI, a Geographic Information System (GIS) attributes the increase in UHI to building height and albedo, so they developed ArcUHI, a tool that combine GIS and machine learning algorithms, to model Surface UHI and predict LST with high accuracy, to adopt mitigation strategies that can be used to guide strategic actions, such as the adoption of green roofs and walls, reflecting coatings, or cool pavements/roofs, to reduce the heat absorption capacity of built surfaces as reviewed by others [15]. By incorporating these elements, planners can create cities that are both environmentally sustainable and favorable to human-well-being, while also considering socio-demographic factors.

In Mexico, the National Projects for Research and Incidence (PRONAII) managed by the National Council of Humanities, Sciences, and Technologies (abbreviated CONAHCyT) integrates scientific-technical expertise to facilitate cooperation between academic and private or public entities [16]. This research initiative include metropolitan institutes of research and planning, enhancing the use of official data resources to tackle urban climate change and reach the UN Sustainable Development Goals for sustainable cities and communities, and fostering National Development Plans, addressing social, environmental, and demographic issues by suggesting multicriteria studies to mitigate the Urban Heat Island effects.

The present work addresses the constraints of climatic information provided by traditional meteorological stations in the national meteorological system of Mexican cities. The climatological data mentioned above are often standardized to examine heat exposure in urban areas. However, unlike remote sensing instruments, they lack the ability to offer a comparative geospatial resolution for conducting temporal analysis to assess the intensity of urban heat islands and the changes in land surface temperature within urban areas. The primary objective of this study derived from PRONAII was to use spectral images from the Landsat 8 satellite to compare and assess the urban land cover and Surface Urban Heat Island effects of the City of Ensenada, Baja California. Specifically, the study focused on comparing average typical summer days in 2019 and 2023.

2. Method

This research was conducted in the sparsely populated city of Ensenada, Mexico. The coastal city is located at latitude 32° 12’ 10” N and longitude 116° 53’ 03” W, bordering the Pacific Ocean. It covers an area of 71.446 km^2, has 119,796 inhabited dwellings, and an average occupancy rate of 3.16 inhabitants per urban dwelling. The average population density is 9 residents per square kilometer (residents/sq.km) [17] that can reach 58.46 residents/sq.km in the northeast sector of the city [18]. The population is projected to grow by 66,226 more people by 2030 compared to 2020, with an annual growth rate of 0.98% according to the State Development Planning Committee (COPLADE) [19]. The maximum housing land use intensity allowed in the 2034 urban strategic plan is 182 inhabitants per hectare (people/ha) for single-family dwellings and 500 people/ha for multi-family dwellings [20]. The lack of an adequate regulation plan will result in significant social and environmental impacts, including the degradation and disappearance of green infrastructure. Additionally, the disorderly growth of the city in peripheral areas will lead to an increase in informal housing [21]. The climate in Ensenada is classified as BSk (cold semi-arid climate) according to the Köppen-Geiger climate classification system. This classification refers to a cold semi-arid climate, which is characterized by wet, rainy, and cold winters, as well as hot and dry summers [22].

For the land cover analysis, three primary climatic indicators were chosen: NDVI, LST, and SUHI. NDVI is a numerical indicator that represents the amount of vegetation on the surface; it is measured on a scale from -1 to 1, where negative values imply high reflectivity and positive values indicate the presence of vegetation [23-24]. On the other hand, the LST is influenced by factors such as time, day, ground cover, and meteorological conditions, causing its readings to fluctuate, high LST readings suggest the presence of warm surfaces, whereas low values are typically linked with vegetated areas, water bodies or cool spots in the city [25]. The SUHI phenomenon pertains to the variation in LST caused by the absorption and emission of heat by urban surfaces [26]. It is employed through different methodologies to extract and refine leveraged satellite data in order to assess the heat island intensity [27].

Remote sensing techniques were utilized to estimate the intensity of NDVI, LST, and SUHI. This estimation was carried out through a 6-stage process, as seen in Figure 1. The first stage of the research aimed to identify the typical extreme summer day for 2019 and 2023. This was done

by analyzing ambient temperature oscillation and mean temperature, which involved calculating the monthly total of the absolute differences between the daily average dry bulb temperature (DBTd-avg) and the daily average oscillation (OSCd-avg). The Landsat 8 satellite spectral imagery from the United States Geological Survey (USGS) earth explorer database [28] of September 05, 2019, and August 22, 2023, were selected based on the usual harsh weather conditions, cloud cover, and precipitation. The Operational Land Imager (OLI) and relevant Band 4 (Red): 0.64 – 0.67 micrometers (μm) and Band 5 (Near-Infrared, NIR): 0.85 – 0.88 micrometers (μm), were utilized to capture multispectral imagery in different wavelength bands and estimate NDVI. At the same time, Band 10: 10.60 – 11.19 micrometers (μm) employ the Thermal Infrared Sensor (TIRS) to capture earth´s surface infrared radiation.

In order to conduct the SUHI evaluation (See Eq.7), it was previously necessary to calculate the $L\lambda$: spectral radiance (See Eq. 1), and LST (See Eq. 6), which was derived from the spectral indices of emissivity (ε) (See Eq.5) and brightness temperature (T_B) (See Eq.2). The value of ε was determined by using Equation 5, which is dependent on the NDVI. Equation 4 was used to calculate the NDVI by measuring the reflectance of the RED and NIR bands. The estimation of T_B was performed using spectral radiance, as shown in Eq. 2. The approach mentioned above was computed using the GIS software ArcGIS v10.8.2 by analyzing the spectral imagery, ArcGIS is considered as a decision support tool, widely used for its spatial data integration and multi-criteria decision-making enhancement [29] the process of determining these national responsibilities and conservation priorities is time intensive when considering many species across geographic scales.

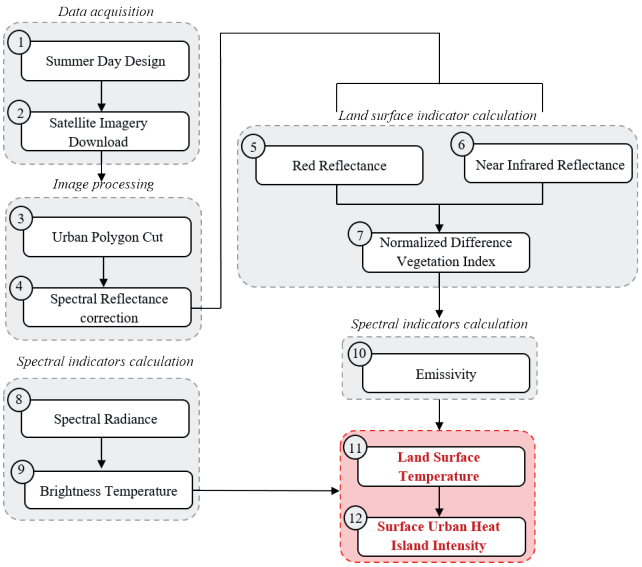

Fig. 1. Methodological workflow for calculating LST and SUHI.

Table 1. Different spectral indices used for calculation.

Index	Equation		Ref
L_λ	$M_L \times DN_{band} + A_L$	(1)	[30]
T_B	$\frac{K_2}{ln\left(\frac{K_1}{L_\lambda}+1\right)}$	(2)	[31]
ρ_λ*	$\frac{\rho}{sin(\theta\pi\ /\ 180)}$	(3)	[30]
NDVI	$\frac{(\rho_{NIR}-\rho_{red})}{(\rho_{NIR}+\rho_{red})}$	(4)	[32]
ε_λ	$\{\varepsilon_s\ \ \varepsilon_s\ \ \varepsilon_s\} = \{\varepsilon_s,\ \ \varepsilon_{(m,)}\ \ \varepsilon_v\}$	(5)	[33]
LST	$\left(\frac{T_B}{1+\left(\frac{\lambda T_B}{\alpha}\right) ln\ \varepsilon}\right) - 273.15$	(6)	[34]
SUHI	$\frac{LST_i - LST_{min}}{LST_{max} + LST_{min}}$	(7)	[35]

Note: Where: M_L: radiance multiplicative scaling factor, A_L: radiance additive scaling factor, DN_{band}: raw band digital numbers, α: surfaces radiation constant adjustment, ε_s: emissivity bare soil (NDVI<0.2), ε_v: emissivity vegetation (NDVI>0.5), ε_m: emissivity mixed areas (NDVI>0.2 & NDVI<0.5), *Spectral range dependent index (adapted), being Red Reflectance: ρ_{red} and NIR Reflectance: ρ_{NIR}.

After normalizing the skewed SUHI data, the current approach utilized Jenks' natural breaks data classification technique to assess the intensity of the phenomena. This optimization method allows for the grouping of data into clusters and optimizes the distinction between groups minimizing the variance between them to facilitate normalization across multiple dimensions. In order to achieve this objective and provide natural data groupings, a 5-class scale was employed, utilizing the categories suggested by Zhang [36].

3. Results and discussion

In order to analyze the distribution pattern of the Surface Urban Heat Island in Ensenada, we obtained a series of maps showing the LST and SUHI on a typical extreme summer day in 2019 and 2023. These maps were generated using data from the Landsat 8 satellite, technical assumptions regarding the urban overheating in relation to typical physical properties, such as emissivity (ε) variations across the urban surface -comprising different building materials (0.85 – 0.95), asphalt pavements (0.90 – 0.95), and vegetation (0.7 – 0.95)- were appropriately calculated to ensure stability and reliability. Atmospheric conditions, including clear-sky conditions with normal atmospheric transmissivity, and Aerosol Optical Depth (AOD) values were also accounted for to maintain consistency and accuracy in processing the city's heterogene-

ity [37]. In terms of satellite thermal bands, the radiance multiplicative scaling factor for Band 10 (0.000342) and the radiance additive scaling factor (0.1) were considered. Additionally, the reflectance multiplicative scaling factor (0.00002) and the reflectance additive scaling factor (0.1) for Bands 4 and 5 were also taken into account. There are notable disparities in the spatial arrangement of LST in the designated region between the years 2019 and 2023. According to the data presented in Figure 2a, the LST trend in 2019 exhibits a greater accumulation of high temperatures in the northern and northeastern regions of the city. These temperatures can reach values as high as 38.65 °C. The eastern urban edge of the city is undergoing rapid and uncontrolled expansion, leading to the formation of densely populated areas with limited water bodies and vegetation. In contrast, the western section of the city exhibits LST values of 23.64 °C as a result of its close proximity to the water.

Conversely, the year 2023 had a rise in the distribution of maximum temperatures, primarily centered in the central and northeastern areas of the city, reaching a peak of 40.23 °C. Similarly, it was noted that in 2023, the regions with the lowest LST are situated in the northwest. These areas have a minimum LST value of 22.89 °C, which can be attributed to their closeness to bodies of water and the cooling effect of wind as a convective mechanism (Fig. 2b).

The classification of SUHI intensity grade was defined by correlating these pixel values with land surface temperatures, to classify SUHI intensity based on the distribution and concentration of temperature anomalies across the urban landscape from 2019 and 2023, taking into account the distribution of temperature data for each year observed. This resulted in a five-category scale, as shown in Table 2.

Table 2. Classification of the degree of intensity of SUHI

SUHI 2019	SUHI 2023	SUHI Intensity
<0.40	<0.37	I. Cool Island
0.41-0.55	0.38-0.50	II. Weak SUHI
0.56-0.66	0.51-0.60	III. Moderate SUHI
0.67-0.75	0.61-0.70	IV. Strong SUHI
>0.75	>0.71	V. Extreme SUHI

The SUHI intensity estimation findings can be seen in Fig. 2c. In 2019, there was an extreme SUHI (V) in the northeast and southeast regions of the city, with an intensity ranging from 0.70 to 1. In contrast, the southeastern region exhibited a significant SUHI effect, with intensities ranging from 0.56 to 0.66 and 0.67 to 0.75, respectively. On the other hand, this investigation also discovered a Cool island located in the southwest area, characterized by an intensity ranging from 0 to 0.40.

In 2023, the intensity of the urban heat island (V) is highest in the center and northern areas of the city, with values exceeding 0.71. In contrast, the southern zone of the city experiences mostly significant urban heat island effects (IV), with values ranging from 0.61 to 0.70. The primary fluctuations in SUHI intensity are observed in the northeastern and southeastern regions. These changes can be attributed to disruptions on the Earth's surface, resulting in variations in NDVI of up to 0.02 (See Fig. 2d).

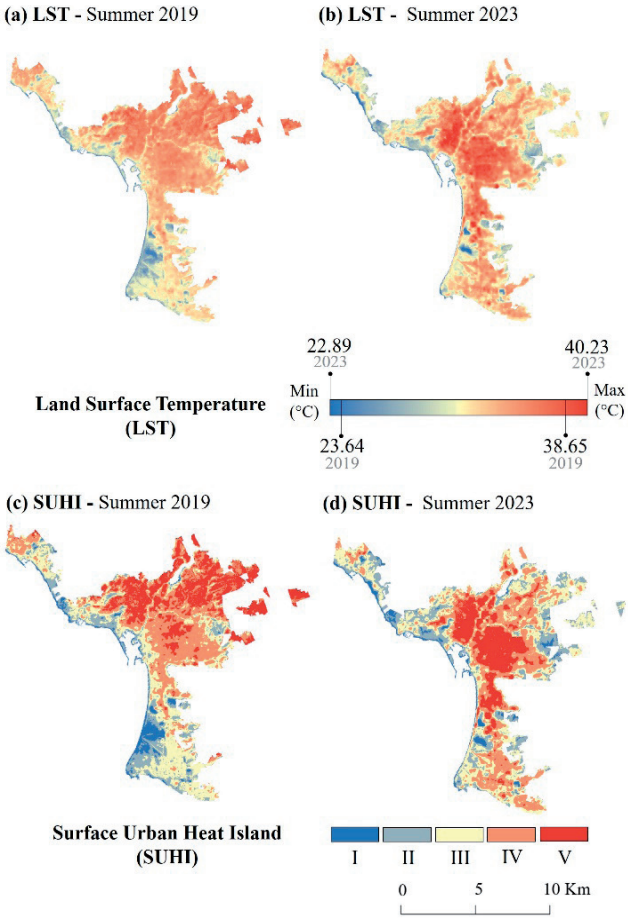

Fig. 2. LST - SUHI 2019-2023 spatial distribution.

Fig. 3a displays the results of the relative differences in the extreme temperatures of LST between the years 2019 and 2023. The National Institute of Statistics and Geography (INEGI) defined the Basic Geostatistical Area (AGEB) as the spatial unit of analysis for the census in Mexico. The urban area of Ensenada encompasses a total of 269 AGEBs.

According to the map, 42.37% of the AGEBs (114 AGEBs) experience a rise in surface temperature. The temperature fluctuates between 0.06 to 4.35 °C in the central and southern parts of the city. In 2023, there is an average increase of 1.5 °C in severe temperatures compared to 2019 in the city. The rise is due to a reduction in the NDVI index by 24.16%, impacting 65 out of the 269 AGEBs that were examined. In contrast, the northeastern region observed a decline in temperature, ranging from 1 to 6 °C.

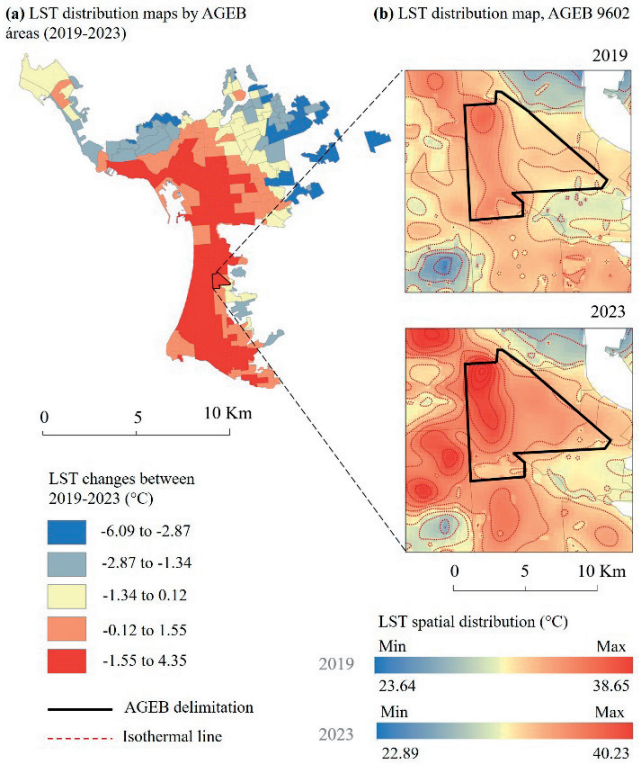

Fig. 3. AGEB LST 2019-2023 comparative analysis.

Similarly, AGEB 9602 characterized by a mixed land use (commercial and services), presents the typical features of an LCZ-3 (compact low rise), in the eastern part of the AGEB, characterized by the presence of residential buildings, and an LCZ-7 (lightweight low rise), in the western part of the AGEB, attributable to the commercial zone. This region also presents a large extension of impervious surfaces, traffic affluence, and lack of green infrastructure, which led to a greater increase in temperature, coinciding with the findings presented by Ejiagha [12], who attributes the LST increase in residential zones to the extensive impervious surfaces, and the high construction density. In 2019, the maximum recorded LST was 38.65 °C, while in 2023, it reached 40.23 °C, indicating a temperature increase of 4.35 °C. The rise in temperature can lead to heat stress episodes, which have varying impacts on health depending on age and pre-existing illnesses. These effects are particularly pronounced in individuals with heart disease, children, and adults over the age of 60, and the female population [38]. The heat-sensitive population in this AGEB is spread among the following age groups: The female population accounts for 52.9% of the total population of 2,857 inhabitants. Among this group, 19.42% are aged 0 to 14 years and 8.64% are adults older than 60 years. Based on the information provided in Figure 3b, AGEB 9602 displays isotherms corresponding to different temperature increments. These isotherms have a mostly west-northwest orientation and cover an area of 0.02 square kilometers. The isotherm exhibits a steady variability, characterized by a gradual rise in temperature from the northwest and a subsequent decrease towards the east of the AGEB. On the other hand, Fig. 3a displays isotherms that are oriented in a northwest-southwest direction, indicating that the isotherm surface expanded by 0.13 km² towards the southwest area.

Based on the information provided in Figure 3b, AGEB 9602 displays isotherms corresponding to different temperature increments. These isotherms have a mostly west-northwest orientation and cover an area of 0.02 square kilometers. The isotherm exhibits a steady variability, characterized by a gradual rise in temperature from the northwest and a subsequent decrease towards the east of the AGEB. On the other hand, Fig. 3a displays isotherms that are oriented in a northwest-southwest direction, indicating that the isotherm surface expanded by 0.13 km² towards the southwest area.

Fig. 4. Street-level view and satellite overview. Google Earth

The aforementioned phenomenon can be linked to the decline in green infrastructure, as indicated by a 0.06 fall in NDVI caused by the expansion of urban areas. As depicted in Figure 4, this AGEB exhibits compact and low-rise structures, which are indicative of LCZ - 3 (Compact low-rise). Similarly, in the hottest temperature zone, there is a significant presence of extensive pavements and materials like steel and concrete, which are characteristic of LCZ - 8 (Large Low-rise). The urban plan in this area follows a north-south orientation for main highways and an east-west orientation for subsidiary and local roads. According to Manni [39], the east-west orientation is regarded as undesirable since it results in a longer exposure to sun radiation and, consequently, a rise in the mean radiant temperature. In addition, the flow of vehicles on roads significantly impacts the increase in LST, influenced by factors such as heat and pollutant emissions, and interactions with paved surfaces. These effects intensify the urban heat island phenomenon, especially in areas with high traffic density. In the case of AGEB 9602, it is observed that the area is bordered by main and secondary roads with vehicular traffic volumes reaching up to 2,600 and

839 vehicles per hour [40], respectively. This exacerbates the urban heat island effect due to the high concentration of vehicles and their influence on heat transfer in the urban environment.

4. Conclusions and Recommendations

This study utilized remote sensing techniques to evaluate the magnitude of the SUHI in Ensenada, Mexico, from 2019 to 2023 as a relevant spatial tool for smart urban planning. The main findings are summarized below:

- Elevated LST: The analysis indicated an increase in LST over a substantial area (42.37%) of Ensenada from 2019 to 2023. The mean temperature rise was 1.5 degrees Celsius.
- Changing the intensity of the SUHI: The study documented a change in the intensity of the SUHI that occurred in different locations. The northeastern region had a decline in temperature, but the central and southern zones of the city observed an increase that must be addressed under a LCZ typological analysis, due to its density aspects.
- AGEB 9602 had the highest temperature rise, with a substantial increase of 4.35 °C. This region exhibits a significant concentration of population groups that are particularly vulnerable to heat (such as children, elderly individuals, and females) and is deficient in terms of green infrastructure, failing to provide adequate evapotranspiration, a higher albedo effect, shaded areas to reduce the overall heat, and the reduction of heat-absorbing surfaces.
- The urban morphology of AGEB 9602 is a contributing factor to the increasing temperatures. The presence of compact low-rise buildings and broad asphalt pavements exacerbates the urban heat island effect by trapping heat due to the high solar exposure during the day, which can reach an annual total solar radiation that exceeds 2,000 kWh/m^2/year in the 25-35° tilt angle for street surfaces in the region [41].
- The decline in NDVI values, which indicates a loss in vegetation, is consistent with regions facing rising temperatures. This emphasizes the vital need for green infrastructure in moderating the urban heat island effect in urban configurations with scarce vegetation.

These findings allow for the following recommendations to be made for urban planners and architects, local and national government authorities, and public health officials, as well as for key participants in the private sector such as real estate developers, Non-Governmental Organizations (NGOs), and academic and research institutions:

- The development and implementation of green infrastructure as territorial reserves in strategic districts with critical microclimatic conditions. A robust integrated urban policy to enhance the presence of environmentally friendly areas within the urban landscape, including the distribution of parks, gardens, and green roofs. This will aid in the regulation of temperatures and deliver a cooling impact known as cooling islands.
- Urban Design Modifications: Consider updating urban design plans to include elements that reduce heat absorption. This may entail integrating additional shade from trees and buildings, using lighter-colored reflective pavements, and advocating for a north-south building orientation.
- Perform a sensitivity assessment to determine places with a high likelihood of experiencing heat stress and identify the populations that are most vulnerable to its impacts. This will enable precise interventions and public health initiatives, including cardioprotective spaces that must be strategically distributed in specific urban districts with high exposure, like in the case of AGEB 9602.
- Surveillance and assessment: Utilize remote sensing techniques to consistently monitor the intensity of LST and SUHI. This will provide an ongoing assessment of the efficacy of adopted strategies.
- Geographical Information System analysis using remote sensing enables the smooth integration of data, predictive analytics, and improved decision-making. In the future, IoT-based ecosystems will provide interoperability with Urban Building Energy Models (UBEM) and digital twins (DTs) to evaluate important aspects of preventing the increasing heat-related mortality rate and energy poverty.
- In future technological applications, the Internet of Things (IoT) can be integrated into the evaluation of the spatio-temporal distribution of urban overheating in real time for multi-criteria decision-making (MCDM) in GIS-based smart urban planning. Remote sensing techniques can be used to estimate the urban centrality of residential areas in relation to tourist clusters, industrial zones, cultural heritage districts, multimodal mobility hubs, traffic hubs, and short-term territorial reserves. This allows for the implementation of strategic actions and local smart grids to promote efficient governance, public safety and security, waste management, water security, epidemiological prevention, and e-services for urban ecosystems.

Finally, it is crucial to include a demographic analysis of AGEB in urban planning schemes that consider the environmental factors of vulnerability and exposure when designing urban areas. This should include the establishment of Enhanced Urban Green places, often known as urban forests, as well as Cooling Centers that provide refuge for vulnerable people during periods of high heat. Moreover, it is important to promote Public Awareness Campaigns and solutions for prevention. Furthermore, it is essential to take into account heat health warning systems, water delivery, accessible healthcare, and transportation services.

5. References

[1] United Nations Department Economic and social affairs, “Population Facts,” Life expectancy at birth increasing in less developed regions.

[2] UNCTAD, "UN Trade and Development Handbook of statistics: Total and urban population," Genova, 2024.

[3] UN-Habitat, "Envisaging the Future of Cities," 2022.

[4] C. R. de Almeida, A. C. Teodoro, and A. Gonçalves, "Study of the urban heat island (Uhi) using remote sensing data/techniques: A systematic review," *Environ. - MDPI*, vol. 8, no. 10, pp. 1–39, 2021, doi: 10.3390/environments8100105.

[5] U.S. Environmental Protection Agency, "Urban Heat Island Basics," Washington, 2008. doi: 10.1109/IICPE.2016.8079546.

[6] IPCC, "IPCC Fourth Assessment Report: Climate Change 2007," Zurich, 2007. [Online]. Available: https://archive.ipcc.ch/publications_and_data/ar4/wg1/en/ch3s3-2-2-2.html

[7] G. Levermore, J. Parkinson, K. Lee, P. Laycock, and S. Lindley, "The increasing trend of the urban heat island intensity," *Urban Clim.*, vol. 24, pp. 360–368, 2018, doi: 10.1016/j.uclim.2017.02.004.

[8] I. D. Stewart and T. R. Oke, "Local climate zones for urban temperature studies," *Bull. Am. Meteorol. Soc.*, vol. 93, no. 12, pp. 1879–1900, 2012, doi: 10.1175/BAMS-D-11-00019.1.

[9] A. Karimi, P. Mohammad, A. García-Martínez, D. Moreno-Rangel, D. Gachkar, and S. Gachkar, *New developments and future challenges in reducing and controlling heat island effect in urban areas*, vol. 25, no. 10. Springer Netherlands, 2023. doi: 10.1007/s10668-022-02530-0.

[10] C. Wu *et al.*, "Spatiotemporal evolution of urbanization and its implications to urban planning of the megacity, Shanghai, China," *Landsc. Ecol.*, vol. 38, no. 4, pp. 1105–1124, 2023, doi: 10.1007/s10980-022-01578-7.

[11] X. Chen, Y. Xu, J. Yang, Z. Wu, and H. Zhu, "Remote sensing of urban thermal environments within local climate zones: A case study of two high-density subtropical Chinese cities," *Urban Clim.*, vol. 31, no. July 2019, p. 100568, 2020, doi: 10.1016/j.uclim.2019.100568.

[12] I. R. Ejiagha, M. R. Ahmed, Q. K. Hassan, A. Dewan, A. Gupta, and E. Rangelova, "Use of remote sensing in comprehending the influence of Urban landscape's composition and configuration on land surface temperature at neighbourhood scale," *Remote Sens.*, vol. 12, no. 15, 2020, doi: 10.3390/RS12152508.

[13] M. Mohamed, A. Othman, A. Z. Abotalib, and A. Majrashi, "Urban heat island effects on megacities in desert environments using spatial network analysis and remote sensing data: A case study from western Saudi Arabia," *Remote Sens.*, vol. 13, no. 10, 2021, doi: 10.3390/rs13101941.

[14] D. Jato-Espino, C. Manchado, A. Roldán-Valcarce, and V. Moscardó, "ArcUHI: A GIS add-in for automated modelling of the Urban Heat Island effect through machine learning," *Urban Clim.*, vol. 44, no. June, 2022, doi: 10.1016/j.uclim.2022.101203.

[15] P. K. Diem *et al.*, "Remote sensing for urban heat island research: Progress, current issues, and perspectives," *Remote Sens. Appl. Soc. Environ.*, vol. 33, no. October 2023, p. 101081, 2024, doi: 10.1016/j.rsase.2023.101081.

[16] CONAHCYT, "PRONACES," National Project for Research and Incidence.

[17] Instituto Metropolitano de Investigación y Planeación de Ensenada, "Anuario estadistico municipal de Ensenada [in spanish]," Ensenada, 2018.

[18] Gobierno Municipal, *Plan estratégico municipal de Ensenada. Vision 2034 [in spanish]*, no. 66. Mexico, 2020.

[19] COPLADE, "Población de los Municipios de Baja California 2013-2030," *Año*, vol. 4, pp. 1–7, 2013.

[20] Instituto Metropolitano de Investigación y Planeación de Ensenada, *Proyecto Programa de desarrollo Urbano del Centro de Población de Ensenada PDUCPE 2024-2036 [in spanish]*. Mexico, 2024.

[21] Instituto Metropolitano de Investigación y Planeación de Ensenada, *Proyecto Programa de desarrollo Urbano del Centro de Población de Ensenada PDUCPE 2020-2030 [in spanish]*. Mexico: IMIPENS, 2022.

[22] M. Kottek, J. Grieser, C. Beck, B. Rudolf, and F. Rubel, "World map of the Köppen-Geiger climate classification updated," *Meteorol. Zeitschrift*, vol. 15, no. 3, pp. 259–263, 2006, doi: 10.1127/0941-2948/2006/0130.

[23] S. Guha and H. Govil, "Land surface temperature and normalized difference vegetation index relationship: a seasonal study on a tropical city," *SN Appl. Sci.*, vol. 2, no. 10, pp. 1–14, 2020, doi: 10.1007/s42452-020-03458-8.

[24] S. Garai *et al.*, "Assessing correlation between Rainfall, normalized difference Vegetation Index (NDVI) and land surface temperature (LST) in Eastern India," *Saf. Extrem. Environ.*, vol. 4, no. 2, pp. 119–127, 2022, doi: 10.1007/s42797-022-00056-2.

[25] P. Rajagopal, R. S. Priya, and R. Senthil, "A review of recent developments in the impact of environmental measures on urban heat island," *Sustain. Cities Soc.*, vol. 88, no. May 2022, p. 104279, 2023, doi: 10.1016/j.scs.2022.104279.

[26] P. Smith Guerra, O. Peralta Trigo, P. Sarricolea Espinosa, F. Thomas Cabrera, and O. Meseguer-Ruiz, "Climate-sensitive planning. Opportunities through the study of LCZs in Chile," *Build. Environ.*, vol. 242, no. February, p. 110444, 2023, doi: 10.1016/j.buildenv.2023.110444.

[27] M. Zargari, A. Mofidi, A. Entezari, and M. Baaghideh, "Climatic comparison of surface urban heat island using satellite remote sensing in Tehran and suburbs," *Sci. Rep.*, vol. 14, no. 1, pp. 1–23, 2024, doi: 10.1038/s41598-023-50757-2.

[28] U.S. Geological Survey, "Science for a changing world." Accessed: Jul. 18, 2024. [Online]. Available: https://earthexplorer.usgs.gov/

[29] Y. P. Lin *et al.*, "A GIS-based policy support tool to determine national responsibilities and priorities for biodiversity conservation," *PLoS One*, vol. 15, no. 12 December, pp. 1–23, 2020, doi: 10.1371/journal.pone.0243135.

[30] A. García-Haro, "Guide for calculate the basic remote sensing indices in ArcGIS and QGIS. Procedure, authors and general notes during calculation," 2019. [Online]. Available: https://upcommons.upc.edu/bitstream/handle/2117/184167/Guia_RemoteSensing_2019.pdf

[31] U.S. Geological Survey, "Using the USGS LandsAt Level-1 Data product," Landsat missions. [Online]. Available: https://www.usgs.gov/landsat-missions/using-usgs-landsat-level-1-data-product

[32] J. Weier and D. & Herring, "Measuring Vegetación (NDVI & EVI)," NASA Earth Observatory. [Online]. Available: https://earthobservatory.nasa.gov/Features/MeasuringVegetation/measuring_veg%0Aetation_1.php%0D

[33] J. A. Sobrino, J. C. Jiménez-Muñoz, and L. Paolini, "Land surface temperature retrieval from LANDSAT TM 5," *Remote Sens. Environ.*, vol. 90, no. 4, pp. 434–440, 2004, doi: 10.1016/j.rse.2004.02.003.

[34] D. A. Artis and W. H. Carnahan, "Survey of emissivity variability in thermography of urban areas," *Remote Sens. Environ.*, vol. 12, no. 4, pp. 313–329, 1982, doi: 10.1016/0034-4257(82)90043-8.

[35] A. Mathew, S. Khandelwal, and N. Kaul, "Investigating spatial and seasonal variations of urban heat island effect over Jaipur city and its relationship with vegetation, urbanization and elevation parameters," *Sustain. Cities Soc.*, vol. 35, no. April, pp. 157–177, 2017, doi: 10.1016/j.scs.2017.07.013.

[36] Y. Zhang *et al.*, "Spatiotemporal characteristics of the surface urban heat island and its driving factors based on local climate zones and population in beijing, china," *Atmosphere (Basel).*, vol. 12, no. 10, 2021, doi: 10.3390/atmos12101271.

[37] Z. L. Li *et al.*, "Satellite-derived land surface temperature: Current status and perspectives," *Remote Sens. Environ.*, vol. 131, pp. 14–37, 2013, doi: 10.1016/j.rse.2012.12.008.

[38] K. L. Ebi *et al.*, "Extreme Weather and Climate Change: Population Health and Health System Implications," *Annu. Rev. Public Health*, vol. 42, pp. 293–315, 2020, doi: 10.1146/annurev-publhealth-012420-105026.

[39] M. Manni *et al.*, "Development and validation of a Monte Carlo-based numerical model for solar analyses in urban canyon configurations," *Build. Environ.*, vol. 170, no. November 2019, p. 106638, 2020, doi: 10.1016/j.buildenv.2019.106638.

[40] IMIPENS, "Estudio de tránsito de tránsito vehicular de la ciudad de Ensenada, B.C.," 2009.

[41] J. F. Armendariz-Lopez, A. Luna-Leon, M. E. Gonzalez-Trevizo, A. P. Arena-Granados, and G. Bojorquez-Morales, "Life cycle cost of photovoltaic technologies in commercial buildings in Baja California, Mexico," *Renew. Energy*, vol. 87, pp. 564–571, 2016.